Systems/Circuits

A VTA to Basal Amygdala Dopamine Projection Contributes to Signal Salient Somatosensory Events during Fear Learning

Wei Tang,[1,2] Olexiy Kochubey,[1] Michael Kintscher,[1] and Ralf Schneggenburger[1]
[1]Laboratory of Synaptic Mechanisms, Brain Mind Institute, School of Life Science, École Polytechnique Fédérale de Lausanne (EPFL), Lausanne, 1015, Switzerland, and [2]Bernstein Center for Computational Neuroscience, Humboldt University of Berlin, Berlin, 10115, Germany

The amygdala is a brain area critical for the formation of fear memories. However, the nature of the teaching signal(s) that drive plasticity in the amygdala are still under debate. Here, we use optogenetic methods to investigate the contribution of ventral tegmental area (VTA) dopamine neurons to auditory-cued fear learning in male mice. Using anterograde and retrograde labeling, we found that a sparse and relatively evenly distributed population of VTA neurons projects to the basal amygdala (BA). *In vivo* optrode recordings in behaving mice showed that many VTA neurons, among them putative dopamine neurons, are excited by footshocks, and acquire a response to auditory stimuli during fear learning. Combined cfos imaging and retrograde labeling in dopamine transporter (DAT) Cre mice revealed that a large majority of BA projectors (>95%) are dopamine neurons, and that BA projectors become activated by the tone-footshock pairing of fear learning protocols. Finally, silencing VTA dopamine neurons, or their axon terminals in the BA during the footshock, reduced the strength of fear memory as tested 1 d later, whereas silencing the VTA-central amygdala (CeA) projection had no effect. Thus, VTA dopamine neurons projecting to the BA contribute to fear memory formation, by coding for the saliency of the footshock event and by signaling such events to the basal amygdala.

Key words: **amygdala; auditory conditioning; dopamine; fear memory; optogenetics; VTA**

Significance Statement

Powerful mechanisms of fear learning have evolved in animals and humans to enable survival. During fear conditioning, a sensory cue, such as a tone (the conditioned stimulus), comes to predict an innately aversive stimulus, such as a mild footshock (the unconditioned stimulus). A brain representation of the unconditioned stimulus must act as a teaching signal to instruct plasticity of the conditioned stimulus representation in fear-related brain areas. Here we show that dopamine neurons in the VTA that project to the basal amygdala contribute to such a teaching signal for plasticity, thereby facilitating the formation of fear memories. Knowledge about the role of dopamine in aversively motivated plasticity might allow further insights into maladaptive plasticities that underlie anxiety and post-traumatic stress disorders in humans.

Introduction

Animals must predict dangers to ensure survival; for this reason, powerful mechanisms of pain sensation and fear learning have evolved in animals (Feinberg and Mallatt, 2017). During auditory-cued fear learning, an innocuous sensory percept, such as a tone (the conditioned stimulus [CS]), acquires a negative emotional valence, and will elicit a defensive behavior after being paired with an aversive stimulus, such as a mild footshock (the unconditioned stimulus [US]) (LeDoux, 2000; Tovote et al., 2015). The amygdala has been identified as a brain structure with an important role in fear learning (Davis, 1992; LeDoux, 2000; Duvarci and Paré, 2014; Tovote et al., 2015). Tone (CS)-driven action potential (AP) firing is increased in many lateral amygdala (LA) and basal amygdala (BA) neurons during and after fear conditioning protocols (Quirk et al., 1995; Amano et al., 2011; Grewe et al., 2017). It is thought that excitatory synapses in the LA that code for the CS undergo LTP, which then drives increased LA neuron AP firing responses upon CS presentation (Rumpel et al., 2005; Sigurdsson et al., 2007; Nabavi et al., 2014). Nevertheless, the nature of the US representation that drives this

Received July 26, 2019; revised Mar. 25, 2020; accepted Mar. 26, 2020.

Author contributions: W.T., O.K., M.K., and R.S. designed research; W.T., O.K., and M.K. performed research; W.T., O.K., and M.K. analyzed data; W.T. wrote the first draft of the paper; W.T., O.K., M.K., and R.S. edited the paper; R.S. wrote the paper.

The authors declare no competing financial interests.

This work was supported by Swiss National Science Foundation (SNSF) 31003A_176332/1 to R.S., SNSF National Competence Center for Research Synapsy, Synaptic Bases of Mental Disease Project 28 to R.S., and EMBO Fellowship ALTF 224-2015 to M.K. Image acquisition was done at the Bioimaging & Optics Platform of École Polytechnique Fédérale de Lausanne (Bioimaging and Optics Platform). We thank Heather Murray, Tess Baticle, and Jessica Dupasquier for expert technical assistance; and Dr. Bernard Schneider (École Polytechnique Fédérale de Lausanne) for help with AAV vector packaging.

Correspondence should be addressed to Ralf Schneggenburger at ralf.schneggenburger@epfl.ch.

https://doi.org/10.1523/JNEUROSCI.1796-19.2020

plasticity is less well known, and both an excitatory drive and neuromodulatory signals likely co-exist to instruct plasticity in the LA and BA (Herry and Johansen, 2014). Thus, depolarizing synaptic inputs coding for the US likely contribute to the induction of associative plasticity because footshock stimulation causes cfos expression in a sparse, but distinct neuronal population in the LA and BA (Gore et al., 2015).

In addition to glutamatergic depolarization of LA and BA neurons, behaviorally salient stimuli, such as footshocks, recruit several neuromodulatory systems, which, among other target areas, project to the BA and LA where they can facilitate the acquisition of threat memories (Johansen et al., 2014). Recent work has shown that both acetylcholine and noradrenaline, acting in the LA and/or BA, facilitate the formation of fear memories (Jiang et al., 2016; Uematsu et al., 2017). We wished to investigate whether dopamine acting in the amygdala might be an additional neuromodulator that facilitates the formation of threat memories.

Dopamine neurons in the midbrain VTA are a heterogenous population that project to the prefrontal cortex (PFC), the nucleus accumbens (NAc), and the amygdala (Asan, 1998; Wise, 2004; Lammel et al., 2011, 2012; Beier et al., 2015). Different pools of dopamine neurons can be involved in both appetitively and aversively motivated behavior. Early evidence for a role of dopamine signaling in the amygdala during aversive learning came from measurements of enhanced dopamine in the basolateral amygdala and in the NAc after stressful stimuli (Young and Rees, 1998; Inglis and Moghaddam, 1999; de Oliveira et al., 2011), and from pharmacological experiments with dopamine receptor antagonists in the amygdala (Lamont and Kokkinidis, 1998; Guarraci et al., 1999; Nader and LeDoux, 1999; Heath et al., 2015). On the other hand, classical studies in monkeys and rats have found a role for VTA dopamine neurons in reward processing (Schultz, 1998; Wise, 2004), and some studies found that VTA dopamine neurons are not activated (Mirenowicz and Schultz, 1996) or even inhibited by aversive stimuli (Ungless et al., 2004; Tan et al., 2012). Thus, a role of dopamine neurons in aversively motivated behavior has remained somewhat controversial, despite evidence from genetic manipulations indicating a role of the dopamine system in aversive learning (Fadok et al., 2009; Zweifel et al., 2011), and despite findings that some dopamine neurons in the VTA are excited by aversive stimuli (Guarraci and Kapp, 1999; Brischoux et al., 2009; Gore et al., 2014; for an insightful early review, see Horvitz, 2000). In the present study, we have used optogenetic methods, *in vivo* optrode recordings, cfos imaging, and circuit mapping techniques to investigate the role of a VTA to BA dopaminergic projection in auditory-cued fear learning.

Materials and Methods

Animals

All procedures with laboratory animals (mus musculus) were authorized by the Service of Consumption and Veterinary Affairs, Canton of Vaud, Switzerland (authorizations 2885.0 and 3274.0). The following mouse lines were used in this study: (1) DAT-internal ribosome entry site-Cre line (B6.SJL-Slc6a3$^{tm1.1(cre)Bkmn}$/J, The Jackson Laboratory, #006660; RRID:IMSR_JAX:006660) called here *DAT^{Cre}* mice (Bäckman et al., 2006); (2) Cre-dependent channelrhodopsin 2 reporter line (Madisen et al., 2012) (B6.Cg-Gt(ROSA)26Sor$^{tm32(CAG-COP4*H134R/EYFP)Hze}$/J; The Jackson Laboratory, #024109; RRID, IMSR_JAX:024109, also known as Ai32) called here *ChR2* mice; (3) Cre-dependent tdTomato reporter mice (Madisen et al., 2010) (B6.Cg-Gt(ROSA)26Sor$^{tm9(CAG-tdTomato)Hze}$/J; RRID, IMSR_JAX:007909, also known as Ai9), called here *tdT* mice; and (4) C57Bl6/J wild-type mice (The Jackson Laboratory, #000664; RRID, IMSR_JAX:000664). All experimental mice were virgin males, group-housed under a 12/12 h light/dark cycle with food and water *ad libitum* until separated into single cages 1 d before surgery.

Viral vectors

For Cre-dependent expression of Arch in DAT$^+$ neurons (see Figs. 4, 5), an AAV1:CBA:FLEX:Arch-GFP vector was used (Addgene, catalog #22222-AAV1; RRID Addgene_22222). In mice for the control groups (see Figs. 4, 5) and for anterograde tracing (see Fig. 1), eGFP expression was driven in DAT$^+$ neurons by an AAV1:CAG:FLEX-eGFP vector (Addgene, catalog #51502-AAV1; RRID Addgene_51502).

Surgery for optic fiber implantation

Male mice of 42-49 d were randomly assigned to a control group or to an Arch group, injected, respectively, with AAV1:CAG:FLEX-eGFP or AAV1:CBA:FLEX:Arch-GFP virus (see above). All other procedures were the same between the control and the test groups. For *in vivo* optogenetic silencing experiments of Figure 4, virus suspension (200-400 nl) was injected unilaterally into the VTA of *DAT^{Cre}* mice, at the following coordinates relative to bregma: anteroposterior −3.3 mm; ML −0.35 mm; DV 4.2-4.6 mm (DV measured from the dura surface). Following this, a single optic fiber was implanted unilaterally above the VTA. A single fiber was used because two fibers would likely have interfered with each other, given the medial position of the VTA. For silencing of DAT$^+$ fibers in the BA or the CeA (see Fig. 5), fibers were placed bilaterally above the BA or bilaterally above the CeA, following a bilateral virus injection into the VTA. The fiber coordinates were as follows: anteroposterior −1.66 mm, ML ±3.35 mm, DV 3.65 mm for BA, or anteroposterior −1.36 mm, ML ±2.85 mm, DV 3.65 mm for CeA (DV measured from the dura surface). Stereotaxic surgeries were done with a model 940 stereotactic instrument (Kopf Instruments).

Fiberoptic implants for *in vivo* optogenetic silencing were custom-made from a 200 μm core/0.39 NA/230 μm outer diameter optic fiber (FT200EMT; Thorlabs) and 1.25 mm outer diameter ceramic ferrules (CFLC230; Thorlabs) as described previously (Sparta et al., 2011). Yellow light was produced by a 561 nm diode pumped solid state laser (MGL-FN-561-AOM, 100 mW, CNI Lasers) equipped with an AOM and an additional mechanical shutter (SHB05T; Thorlabs). The laser power was adjusted to be 10 mW at the exit of the implant tip for each animal.

Behavior

Behavioral experiments were performed after 3-4 weeks of postsurgical recovery. Before behavior testing, mice were habituated to handling and to the head tethering imposed by the optic patch cords. A classical auditory-cued fear memory paradigm was performed in a conditioning chamber of an NIR Video Fear Conditioning Package for Mouse (MED-VFC-OPTO-M, Med Associates; RRID, SCR_016928). The 3 d protocol consisted of the following steps (see Fig. 2*A*): On day 1, the mouse was subjected to a habituation session when six tone blocks (CS) were delivered at pseudo-random intervals in a Context A. Each tone block consisted of 30 beeps (7 kHz, 80 dB, 100 ms long, repeated at 1 Hz for 30 s). On day 2 (the same Context A), each of the 30 s tone blocks was followed by a 1 s electric footshock applied through the metal grid floor of the conditioning chamber (0.6 mA AC). On day 3, four CS tone blocks were delivered in a new Context B. For this, the grid floor was replaced with a smooth white acrylic surface, and a curved wall was installed instead of a square arena used in the Context A. The Context A chamber was wiped before and after each session with 70% ethanol, whereas the Context B chamber was cleaned with a general purpose soap. On some occasions, we tested the retrieval of contextual fear memory on day 4 by monitoring the animal's freezing behavior in Context A for 5 min (see Figs. 4*G*, 5*D*,*H*). Freezing was quantified using VideoFreeze software (Med Associates; RRID, SCR_014574) from the recorded videos of behaving mice (30 frames/s). The freezing level (see Figs. 2, 4, 5) was expressed as the percentage of time the mouse spent freezing during the CS presentation (30-s-long tone block).

Optrode recordings

For recording extracellular spiking activity in the VTA (see Fig. 2), we used a 16-channel amplifier (ME16-FAI-μPA; Multi Channel Systems)

and custom-built microdrive-mounted optrodes. The optrode implantation procedure into the VTA (see Fig. 2) was similar as the VTA optic fiber implantation (see above), with an additional stainless-steel microscrew (Antrin Miniature Specialties) implanted into the skull for grounding. Optrodes were custom-built according to Anikeeva et al. (2011), using four tetrodes placed around a central optic fiber (200/230 µm core/outer diameter, NA 0.5; Thorlabs; see Fig. 2*C*). Tetrodes were made from insulated 17-µm-diameter Pt/Ir wires (California Fine Wire). The tetrodes, and one additional wire for a local reference channel were glued onto the optic fiber fixed inside the 1.25 mm ceramic ferrule (Thorlabs), which was inserted into the movable part of a microdrive (Axona). The free ends of tetrode wires were attached to the pins of a NPD-18-VV-GS micro-connector (Omnetics), which was fixed onto the movable part of the microdrive. To minimize the impedance of the wires, platinum was deposited on the wire tips using platinum black plating solution (Neuralynx) according to manufacturer's manual, and an iontophoretic amplifier (MVCS-01, NPI Electronic). The impedance was measured at 1 kHz in PBS solution using the lock-in function of an EPC-10 patch-clamp amplifier (HEKA Elektronik), and was typically <100 kΩ.

One day before the behavior testing, the optrode was repositioned under ketamine anesthesia (90 mg/g body weight ketamine and 10 mg/g xylazine) to search for opto-tagged units in the VTA by advancing it ventrally from the initial implantation site. The optrode was slowly advanced until light-evoked spikes could be detected at a latency of 2-8 ms (see Fig. 2*D*). We used ChR2 expression in DAT^{+} neurons to optogenetically identify recorded units (DAT^{Cre} x *ChR2* mice); in 1 case (FT6963), a DAT^{Cre} mouse was injected with AAV8:hsyn:FLEX:ChETA-eYFP to drive CheTA expression in DAT^{+} neurons. Opto-tagging was done by delivering short (2–5 ms, 3–10 mW) light pulses at 2 Hz repetition rate, from a 473 nm diode pumped solid state laser (MBL-FN-473, 150 mW; CNI Lasers). The opto-tagging procedure was repeated after each behavior session (without advancing the optrode) to collect light-evoked spikes in response to ~2000 light pulses.

Spike sorting and single-unit analysis

Raw data were recorded with the MC_Rack software (MultiChannel Systems; RRID, SCR_014955) at 40 kHz sampling rate, and was bandpass filtered (0.6–6 kHz) before the analysis. The raw data were converted into HDF5 format using Multi Channel Data Manager software (MultiChannel Systems) and then processed (except the spike clustering) using custom-written routines in IGOR Pro 7.08 (WaveMetrics; RRID, SCR_000325). The voltage traces were bandpass filtered (0.6–6 kHz; fourth-order Butterworth filter), and the stimulation artifacts from electric footshocks (on day 2; that appeared as ~2.8 ms transients repeating at 30 Hz @) were blanked by zeroing under manual control. During opto-tagging, a slow artifact likely related to the local field potentials was sometimes observed. To minimize its effect on spike detection, the average traces were calculated over ~200 subsequent light pulses and then subtracted from each channel. Negative amplitude spikes were detected using a threshold method (typically set at −3.2 SD) on each channel, and the spike timestamp was defined by the largest amplitude event within each tetrode. The light-evoked spikes sampled in a 2-8 ms window after the light pulse onset were clustered separately from the spikes recorded during behavior. Individual spike cutouts (filtered for clustering with a bandpass 0.4–6 kHz filter) were exported into MATLAB (MathWorks; RRID, SCR_001622). The MClust toolbox (David Redish; University of Minnesota) was used to cluster the tetrode spikes by an unsupervised clustering algorithm (KlustaKwik; RRID, SCR_014480) (Rossant et al., 2016) using the spike valley and the principal components PCA1-PCA3 as the clustering parameters. The results were quality-controlled by checking the average spike waveform similarity and visualizing the cluster projections; occasionally, some of the clusters were fused together if they were not well separated. Following this, the quality of the spike cluster isolation was estimated by the isolation distance and L-ratio to control for Type I and Type II errors (Schmitzer-Torbert et al., 2005). Clusters with isolation distance >24 and L-ratio <0.5 were retained for analysis; this reduced the total number of clusters from $n=60$ to 28 (sum of opto-tagged and unidentified units in $N=3$ mice; see Fig. 2*I-K*). Qualitatively similar results as the ones shown in Figure 2 were observed without this quality control step.

Opto-tagged units were identified by matching the average waveforms recorded during the behavior session, with those evoked by the light pulses on each day (see Fig. 2*F,L*, insets). Average waveform matching was also used to follow the units across days. Manual matching of the average waveforms was guided by the maximal value of a metric calculated as follows: $[\mathrm{RMS_i} \cdot (1-\rho_i)]^{-1}$. Here, $\mathrm{RMS_i}$ is the average over four electrodes root mean square of a point-to-point differences between the waveforms of two units, and ρ_i is the average Pearson's correlation coefficient calculated between the waveforms of two units. The experimenter was blind to the spiking pattern of individual units during the behavior sessions until the identity of units (opto-tagged or unidentified, and across days) was determined.

Response types of the units to sensory stimuli were classified according to the following criteria: (1) The unit was considered US-responsive if the time-averaged *z* score during the footshock, calculated from the average poststimulus time histograms of six footshock stimuli, exceeded a value of 2. For negative responses, a threshold of −1.5 was used. (2) For the CS response classification, average *z* scores for the 100-ms-long tones were calculated for all $n=30$ tones in one tone block. A unit was considered CS-entrained if, first, the *z* score did not exceed 2 for at least five of six CS presentations on day 1 (i.e., the unit did not have an innate response to tones), and, second, if at least two of the last three tone presentations on day 2 resulted in a summed *z* score >4 (i.e., tone response increased on day 2 as a result of training), or if at least two tone presentations on day 3 resulted in a summed *z* score >4 (i.e., the tone response was maintained on day 3). Only in $N=3$ of 12 mice could units according to the above quality criteria be followed over at least day 2 and day 3; the response types found in these $N=3$ mice are shown in Figure 2*I-K*.

Retrograde tracing and immunohistochemistry

For retrograde labeling (see Figs. 1*G–M*, 3), AlexaFluor-conjugated cholera toxin subunit B (CTB) was used (CTB-Alexa-647; Thermo Fisher Scientific). CTB was injected into the left BA of a DAT^{Cre} x *ChR2* mouse, and a C57Bl6/J mouse (see Fig. 1), or into the BA of DAT^{Cre} x *tdT* mice (see Fig. 3), at the following coordinates from bregma: RC −1.05 mm, ML 3.25 mm, DV −5.18 mm (250 nl of 0.1% dilution in PBS). Seven days (see Fig. 1) or 23 days (see Fig. 3) after CTB injection, the brains were dissected and processed for histologic analysis.

Immunohistochemistry (see Figs. 1*A–F,I,J*, 3*B,C*) and *post hoc* histology with immunohistochemistry to confirm the viral targeting and optic fiber placement (see Figs. 2, 4, 5) were done according to standard procedures after transcardial perfusion of mice with 4% PFA. The following pairs of primary and secondary antibodies were used. For Figure 1*B*, chicken anti-GFP (Abcam; catalog #13970; dilution 1:1000; RRID:AB_300798), and as secondary antibody, goat anti-chicken Alexa-488 (Thermo Fisher Scientific; catalog #A11039; dilution 1:200; RRID, AB_2534096). For the second channel in Figure 1*B*, we used a rabbit anti-TH antibody (Millipore; catalog #AB152; dilution 1:1000; RRID, AB_390204) and as secondary antibody, goat anti-rabbit Alexa-647 (Thermo Fisher Scientific, catalog #A21244; dilution 1:200; RRID:AB_2535812). For Figure 1*I, J*, ChR2-eYFP was detected with a chicken anti-GFP antibody and the corresponding secondary antibody as stated above. For Figure 3*B,C*, we used a rabbit polyclonal anti-cFos antibody (Synaptic Systems; catalog #226003, dilution 1:1000; RRID:AB_2231974), and as secondary antibody, goat anti-rabbit Alexa-488 (Thermo Fisher Scientific, catalog #A11008; 1:1000 dilution; RRID, AB_143165). In Figure 3*B,C*, the tdTomato fluorescence of DAT^{+} cells of the DAT^{Cre} x *tdT* mice was detected without antibody enhancement. For *post hoc* histology after optrode placement (see Fig. 2*C*) or optogenetic fiber placement (see Figs. 4*E*, 5*B*), we costained with an anti-GFP antibody (to detect ChR2-eYFP, or Arch-eGFP, or eGFP expression; green channel), and with the rabbit anti-TH antibody (red channel), with the antibody combinations detailed

above. Slices were mounted in Dako fluorescence mounting medium (Dako).

Image acquisition

Histologic sections were imaged at the Bioimaging and Optics Platform, École Polytechnique Fédérale de Lausanne. For the immunohistochemistry in Figure 1*B*, images were taken on an upright LSM 700 confocal microscope (Carl Zeiss) with 20×/0.8 NA dry and 40×/1.3 NA oil immersion objectives. The corresponding quantification of eGFP and TH colocalization was performed by using an automated ImageJ routine (provided by Olivier Burri, Bioimaging and Optics Platform, École Polytechnique Fédérale de Lausanne). Retrogradely labeled VTA sections (see Figs. 1*I,J*, 3*B,C*) were imaged with a Slide Scanner (VS120-L100; Olympus) with a 10×/0.4 NA objective. For the analysis of retrogradely labeled VTA neurons in Figure 3, a subset of the sections was reimaged at higher resolution with a confocal microscope (LSM 700, Carl Zeiss; 20×/0.8 NA objective), and the colocalization of three markers was analyzed manually. For the *post hoc* histologic analysis after optrode recordings (see Fig. 2) or after optogenetic experiments (see Figs. 4, 5), slices were imaged with a stitching fluorescence microscope (DM5500, Leica Microsystems) using 5×/0.15 NA or 10×/0.3 NA objectives, or with a Slide Scanner VS120-L100 (Olympus) with a 10×/0.4 NA objective.

Ex vivo *electrophysiology*

For slice electrophysiology, 300-µm-thick slices containing the VTA (cut with a Leica VT1000S slicer; Leica Microsystems), were made from 3- to 4-month-old mice previously injected with AAV1:CBA:FLEX:Arch-eGFP. Whole-cell patch-clamp recordings of VTA neurons were done at room temperature (21°C–23°C) with a K-gluconate-based pipette solution, and a standard bicarbonate buffered extracellular solution. The setup was equipped with an EPC10/2 patch-clamp amplifier (HEKA Elektronik) and an upright microscope (Axioskop 2, Carl Zeiss) with a 60×/0.9 NA water-immersion objective (LUMPlanFl, Olympus). For activation of Arch (see Fig. 4*B*), yellow light pulses were delivered from a high-power LED (Amber CREE XP-EII PC, 595 nm; Cree), coupled into the epifluorescence port of the microscope. The LED was controlled with a Cyclops LED driver (https://open-ephys.org) (Newman et al., 2015). The maximal light intensity used in experiments was estimated to be 1.24 mW/mm^2 at the focal plane. The electrophysiological recordings were analyzed in IgorPro using the NeuroMatic plug-in (Rothman and Silver, 2018).

Experimental design and statistical analysis

No prior sample size calculation was performed. Optogenetic silencing experiments with Arch (see Figs. 4, 5) were usually performed in small "cohorts" of $N = 3$ and $N = 3$ mice for "control group" and "Arch group." Repeating such measured cohorts 2-3 times, giving rise to $N = 6$-8 mice in the control and the Arch group, was found necessary to determine whether silencing induced a significant change in the Arch group compared with the control group.

Biological replicates refer to the number of mice (we then use N) or else to the number of cells (n) as indicated in Results. Sometimes, technical replicates, such as the number of analyzed sections, are also indicated in Results.

Statistical tests on behavioral data were performed using Prism 5 (GraphPad Software; RRID, SCR_002798). The data were expressed as mean ± SEM. For the statistical analysis of the optogenetic silencing data (see Figs. 4*G*, 5*D,H*), a repeated-measures two-way ANOVA was used, followed by a *post hoc* Bonferroni test for multiple comparisons. Additionally, for the analysis of cued retrieval, the freezing data in response to all $n = 4$ tone blocks applied on day 3 were pooled and averaged for each group (see Figs. 4*H*, 5*E,I*); in this case, a two-tailed heteroscedastic two-sample Student's t test was used (referred to as t test in Results). A χ^2 test for trend in Prism 8 was used to analyze the fraction of cfos$^+$ neurons (see Fig. 3*D,E*). Significance levels are reported in Results and are additionally indicated in the figures.

Results

Dopamine neurons of the VTA project to the BA and medial CeA

We first investigated the VTA-amygdala projection anatomically by anterograde and retrograde tracing techniques. We used dopamine-transporter Cre mice (DAT^{Cre}) and injected an AAV vector into the VTA to drive Cre-dependent expression of eGFP (AAV1:CAG:FLEX:eGFP; Fig. 1*A*). Confocal fluorescence images revealed many transduced, eGFP-positive cell bodies within the VTA, which were detected by an anti-GFP antibody (see Materials and Methods). Many of these cell bodies were also positive for TH as revealed by an anti-TH antibody (Fig. 1*B*). Specifically, we found that 81 ± 9% (1060 of 1259) of all TH$^+$ cells in the VTA expressed eGFP ($n = 9$ sections from $N = 3$ mice), and that 98 ± 2% (1060 of 1082) of the eGFP-expressing cells were TH$^+$ ($n = 9$ sections from $N = 3$ mice; Fig. 1*C*). Thus, ~80% of the VTA neurons were infected with the AAV1 vector, and expression was virtually limited to TH$^+$ neurons, demonstrating tight expression control by the Cre-dependent expression vector.

In the amygdala region, we found eGFP-expressing axons in the CeA and in the basolateral nucleus complex (Fig. 1*D*). In the latter, the highest fiber density was found in the BA, whereas the LA received few eGFP-positive fibers (Fig. 1*D*). In the CeA, the medial subdivision (Fig. 1*D*, CeA-m) showed a denser innervation with eGFP-positive fibers compared with the lateral CeA (see also Mingote et al., 2015). Nevertheless, the lateral CeA was densely stained by the TH antibody (Fig. 1*D*, CeA-l), consistent with a catecholaminergic innervation of the lateral CeA from a non-VTA source, as suggested previously (Asan, 1998; Hasue and Shammah-Lagnado, 2002; Matthews et al., 2016). In the BA and the medial CeA, the expression pattern of eGFP$^+$ axons largely overlapped with that of TH (Fig. 1*E,F*). In addition to the BA and medial CeA, TH$^+$ fibers, many of which also expressed eGFP, were found in the amygdalostriatal transition zone (Fig. 1*D*). These data show that DAT-expressing neurons in the VTA send axons to the BA, and to the medial CeA.

We next investigated the location of BA-projecting dopamine neurons in the VTA by using the retrograde tracer CTB-Alexa-647, which was injected into the BA of $DAT^{Cre} \times ChR2$ mice (Fig. 1*G*). The injections were limited to the BA (Fig. 1*H*). Retrogradely labeled neurons were found in the mPFC, the hippocampus, and other brain regions known to provide input to the BA (data not shown). In the VTA, we similarly observed retrogradely labeled neurons (Fig. 1*I,J*). We found that BA projectors were homogeneously distributed over the anteroposterior axis (Fig. 1*K,L*), and mediolaterally as measured by the distance from the midline (Fig. 1*L*). On the other hand, we found more BA projectors in the dorsal half compared with the ventral half of the VTA ($n = 145$ of a total of $n = 160$ neurons were located in the dorsal half; Fig. 1*K*). Thus, we confirm a preferential dorsal localization of BA projectors within the VTA (Baimel et al., 2017). However, we could not confirm a preferential localization of BA projectors in the lateral and posterior parts of the VTA; this might be caused by differences in the BA volumes targeted in the present and in the previous study (Baimel et al., 2017). We found $n = 160$ retrogradely labeled neurons in the mouse illustrated in Figure 1*H-L*. In another mouse, we found $n = 107$ back-labeled neurons in the VTA, and these BA projectors were again homogeneously distributed along the anteroposterior and mediolateral axes (Fig. 1*M*). The number of BA projectors we found here is small compared with the total number of TH-

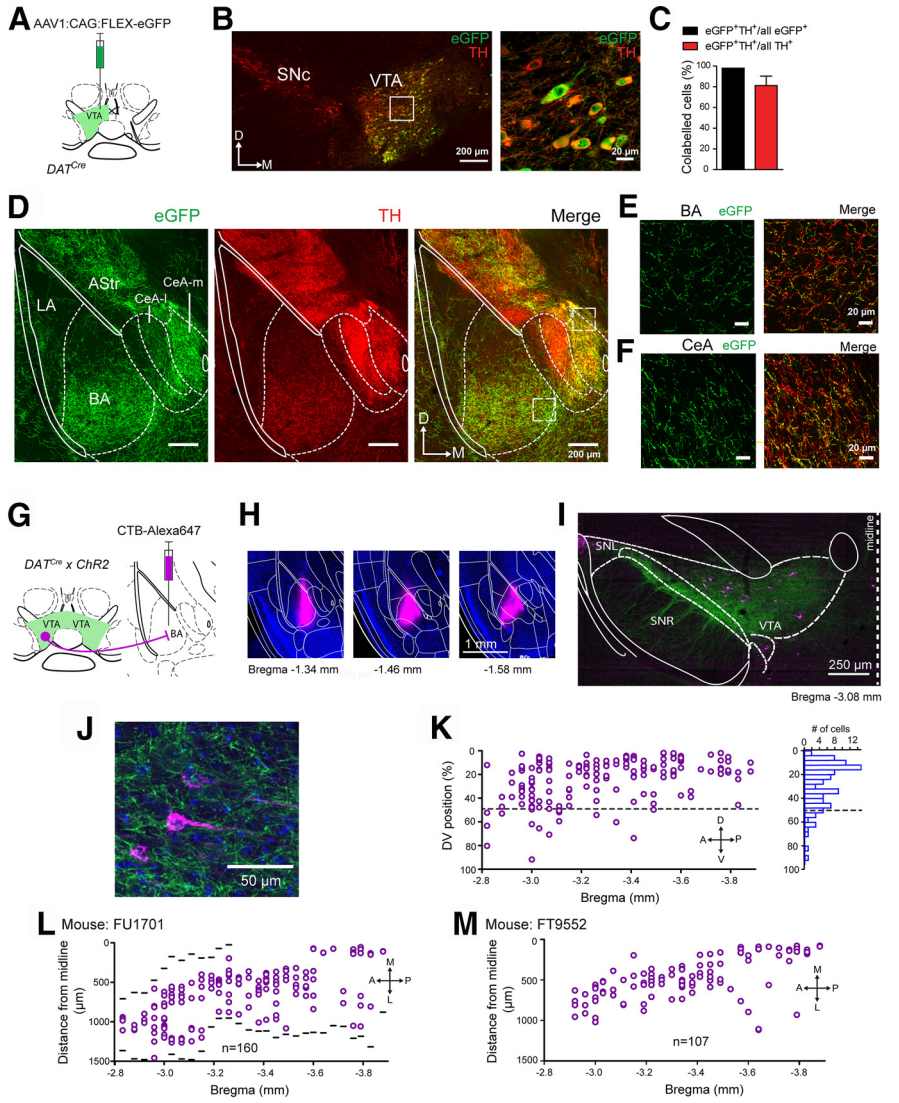

Figure 1. A dopaminergic afferent projection from the VTA to different amygdala subnuclei. ***A***, Schematic of the experimental approach for ***B–F***. An AAV1 vector driving the Cre-dependent expression of eGFP was injected into the VTA of a *DAT*^{Cre} mouse. ***B***, The injection area on the level of the VTA, with eGFP fluorescence (green channel) and the TH immunohistochemistry (red channel). The area indicated by the white box is shown at a higher magnification on the right. eGFP expression is limited to TH$^+$ cells. ***C***, Quantifications of (left) the percentage of eGFP$^+$ cells that were also TH$^+$ among all eGFP$^+$ cells, and (right) the percentage of eGFP$^+$ and TH$^+$-positive cells within all TH$^+$ cells, respectively (mean ± SEM). ***D***, eGFP-expressing axons were observed in the BA, medial portion of the CeA (CeA-m), and in the amygdala-striatal transition zone (AStr), but were largely absent in the LA. White lines and white dashed lines indicate outlines of a mouse brain atlas (Franklin and Paxinos, 2016) overlaid over the images. ***E***, ***F***, Confocal images of eGFP and TH$^+$ fibers in the BA (***E***) and CeA-m (***F***), corresponding to the white dashed boxes in ***D***. ***G***, Schematic of the retrograde labeling approach for ***H-L***. ***H***, Images of the CTB-Alexa-647 (magenta) injection site in the BA at three indicated bregma levels. ***I***, Image of the VTA at the indicated bregma level. Magenta represents neurons back-labeled with CTB-Alexa-647. Green represents GFP (ChR2-eYFP)-positive DAT$^+$ neurons. ***J***, A confocal image of a CTB-Alexa-647-labeled BA-projecting neuron in the VTA. ***K***, Plot of the DV position of CTB-Alexa-647-positive neurons within the VTA (0% represents the most dorsal position), for all sections along the anteroposterior axis of 1 mouse, and the corresponding histogram (right). Note the preferential position of BA projectors in the dorsal half of the VTA. ***L***, Plot of the ML position of CTB-Alexa-647-positive neurons (BA projectors; $n = 160$), for all sections along the anteroposterior axis. Black lines indicate the medial and lateral borders of the VTA. ***M***, Mediolateral position of BA projectors ($n = 107$) from another mouse (C57Bl6) back-labeled by injection of CTB-Alexa-647 into the BA.

positive neurons previously estimated in the A10 area of C57Bl6 mice (~5000) (Nelson et al., 1996); A10 roughly corresponds to the area defined as VTA here. Together, anterograde and retrograde labeling experiments reveal a projection of DAT$^+$ neurons in the VTA to the BA and CeA. The projection to the BA is carried by a quite small subpopulation of relatively evenly distributed neurons in the VTA.

VTA neurons respond to footshocks and acquire CS responses

To investigate the role of VTA dopamine neurons in fear learning, we recorded the activity of these neurons throughout a 3 d fear learning paradigm. During the fear learning protocol, we applied six tone blocks without footshock on day 1. On day 2, the tone blocks coterminated with a 1 s footshock; and on day 3, retrieval of auditory-cued fear memory was assessed by applying $n = 4$ tone blocks alone in a different context (Fig. 2*A*, top; and see Materials and Methods). The example mouse of Figure 2 showed an initial freezing response after it was connected to the optrode cables and released into the fear arena (Fig. 2*A*, arrow). We often observed this behavior in optrode-recorded mice, but not during optogenetic experiments in other mice (see Figs. 4, 5). The mouse illustrated in Figure 2*A–I* developed a strong freezing response on the training day and maintained this level of freezing on the retrieval day (Fig. 2*A*). For the *in vivo* recordings, we used optrodes, which consisted of four tetrode bundles placed around a central optical fiber (Fig. 2*B*,*C*) (Anikeeva et al., 2011). Initial attempts to optogenetically identify BA projectors after expression of ChR2 with retrograde viruses in the BA (herpes simplex virus) were not fruitful, maybe because of the relatively sparse population of BA projectors in the VTA (Fig. 1). We therefore decided to express ChR2 under the DAT promoter using *DAT*^{Cre} × *ChR2* mice, which allowed us to identify a fraction of the recorded units as putative dopamine neurons by optogenetic stimulation (Fig. 2*D*).

During the training day, when tones (CS) were paired with footshock stimulation, a majority of the recorded units responded with an increased AP firing to the footshocks, and acquired an AP firing response to the CS. The example unit shown in Figure 2*E*, *F* (a putative DAT$^+$ dopamine neuron) reliably responded to the footshock (Fig. 2*E*, right). In addition, this unit developed a short-latency response to the tone beeps when these were followed by a footshock on the training day (Fig. 2*E*). The tone response was maintained during the retrieval of threat memory 1 day later (day 3; Fig. 2*F*). In this mouse, $n = 8$ units that fulfilled the quality criteria for unit isolation could be followed through at least day 2 and day 3. In $n = 4$ of these units, a CS response developed during the pairing of the CS with a footshock, whereas other units remained below the criterion for a response

(Fig. 2*G*, pink and gray traces, respectively). Regarding the responses to footshocks, $n = 6$ units in this mouse responded to footshocks, whereas $n = 2$ units did not (Fig. 2*H*, pink and gray traces, respectively). The strength of the AP firing response to each footshock varied in time, but no clear time dependence could be found (Fig. 2*H*).

We next analyzed the various response types in the form of Venn diagrams for each mouse (Fig. 2*I–K*). We made optrode recordings in $N = 12$ mice, but we could only recover useful single units that adhered to the quality criteria in $N = 3$ mice (see Materials and Methods). In these mice, there was a substantial overlap between US responders and CS-entrained units (Fig. 2*I–K*; red and blue areas, respectively). In all 3 mice, opto-tagged units (putative DAT$^+$ neurons) were a subpopulation of US-responding and CS-entrained units (Fig. 2*I–K*, white and yellow areas); and in each mouse, we found a minority of nonresponding units (Fig. 2*I–K*, gray areas). Furthermore, we observed a decrease in AP firing in response to footshocks in $n = 1$ opto-tagged unit (Fig. 2*L*; see Fig. 2*J*, red dashed area), and in $n = 1$ of 20 nonidentified units (Fig. 2*J*, blue dashed circle). Therefore, in this sample, units that responded with a decrease in AP firing were found less often ($n = 2$) than units that responded with an increased firing to footshocks ($n = 21$).

Together, a majority of units recorded in the VTA during the fear learning protocol, among them putative DAT$^+$ neurons, responded with an increased AP firing to the footshocks, and acquired a short-latency response to tones when these were reinforced by a footshock. These results suggest that VTA dopamine neurons play a role in auditory-cued fear learning.

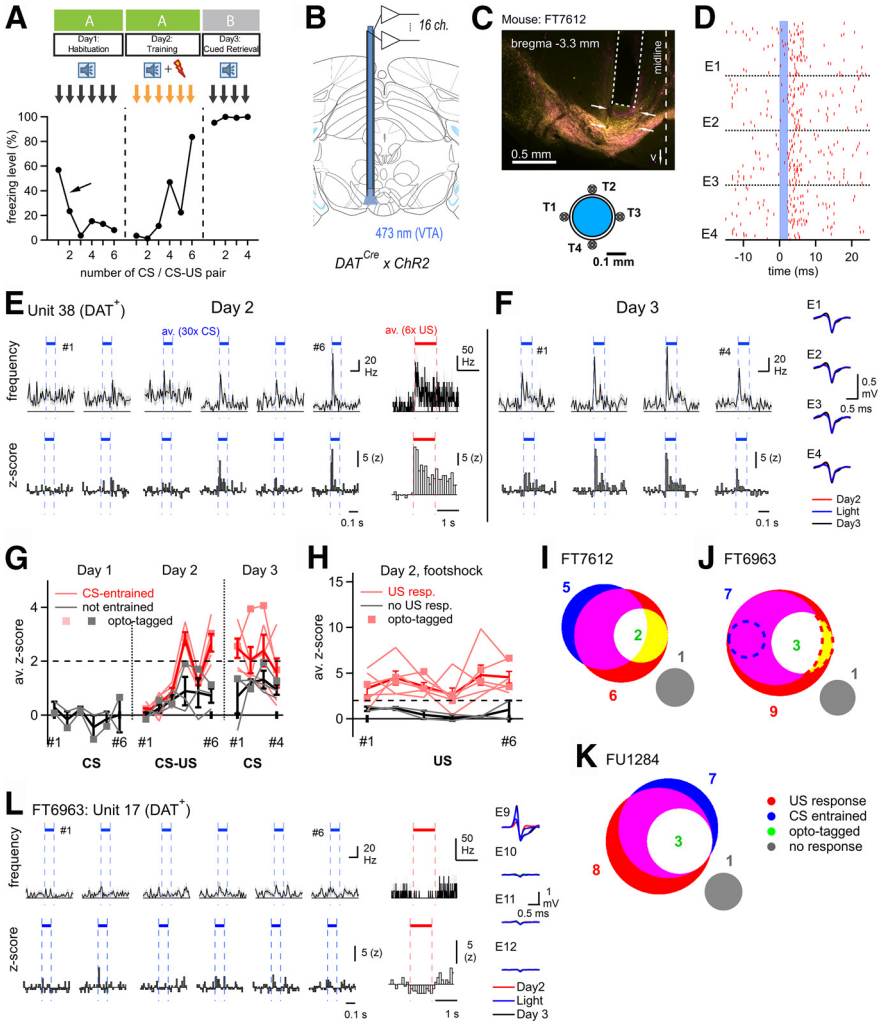

Figure 2. VTA neurons, and among them dopamine neurons, respond to footshocks and acquire CS responsiveness. ***A***, Scheme of the 3 d auditory-cued fear learning protocol (top), and freezing data (bottom) of the example mouse of ***C–I***. ***B***, Schematic drawing of an optrode with 16 recording channels implanted in the VTA of a *DAT^{Cre}* x *ChR2* mouse. ***C***, *Post hoc* histologic image showing the placement of an optrode (dashed line) in the VTA of the example mouse (FT7612) of ***C–I***. The tracks of two tetrodes are visible (arrows). Bottom, Scheme of the arrangement of four tetrodes (T1-T4) around the optical fiber. ***D***, Illustration of optogenetic identification of putative DAT$^+$ units. Raster plot for four electrodes (EI-EIV) of one tetrode, showing unsorted spikes aligned to the onsets of $n = 100$, 2-ms-long laser light pulses (blue shading). Spikes at 2-8 ms after the light pulse were collected and subjected to spike clustering (see Materials and Methods). ***E***, Spiking activity of a single opto-tagged putative DAT$^+$ unit during day 2 (training day). AP frequency (top) and *z* score (bottom) are shown in response to the CS (averages over the $n = 30$ tone presentations for each tone block), as well as in response to footshocks (averages over the $n = 6$ footshock presentations; right). ***F***, Spiking activity of the same unit as in ***E***, in response to CS presentations on day 3 (fear memory retrieval). Right, AP waveforms for the unit shown in ***E***, ***F***. ***G***, ***H***, Responses of all units in mouse FT7612 to tone presentations during days 1-3 (***G***), and to footshocks on day 2 (***H***). The peak *z* score responses were plotted as a function of the tone-block number (CS) or paired CS-US presentation. Pink represents units classified as CS-entrained (***G***) or as US responders (***H***). Gray represents the others. Thick red and black lines indicate average ± SEM across these groups, respectively. Square symbols connected by lines represent DAT$^+$ units identified by optotagging. ***I–K***, Venn-type diagrams showing the number of units in the different response classes and their overlap. ***I***, The data are from the example mouse shown in ***A–H***. Note the overall similar distribution and overlap of response types across the $N = 3$ mice. Two US-responsive units in mouse FT6963 showed reduced AP firing frequencies on the footshock (***J***, dashed areas). ***L***, AP firing response of unit 17 of mouse FT6963 during day 2 of the fear learning protocol. This unit responded with a decreased AP firing frequency to footshock stimulation, and corresponds to the red dashed area in ***J***.

Cfos imaging suggests increased firing of BA projectors during fear learning

We observed with optrode recordings that most sampled units in the VTA, and among them DAT$^+$ neurons, responded with an increased firing to footshocks (Fig. 2). However, we were not able to identify BA projectors, most likely because of the low density of this projection-identified neuronal population in the VTA (see above). Therefore, to further investigate whether BA projectors are among the DAT$^+$ neurons that respond to footshocks, we next used cfos immunohistochemistry, combined with retrograde labeling (Fig. 3). To additionally identify DAT$^+$ neurons, we used *DAT^{Cre}* x *tdT* mice for these experiments. CTB was injected into the left BA of *DAT^{Cre}* x *tdT* mice. Three weeks later, the mice underwent a modified fear learning protocol with a habituation day (application of $n = 6$ tone blocks alone), followed by a training day in which tone blocks were followed by footshocks, or else, tone blocks alone were applied (CS only, as a

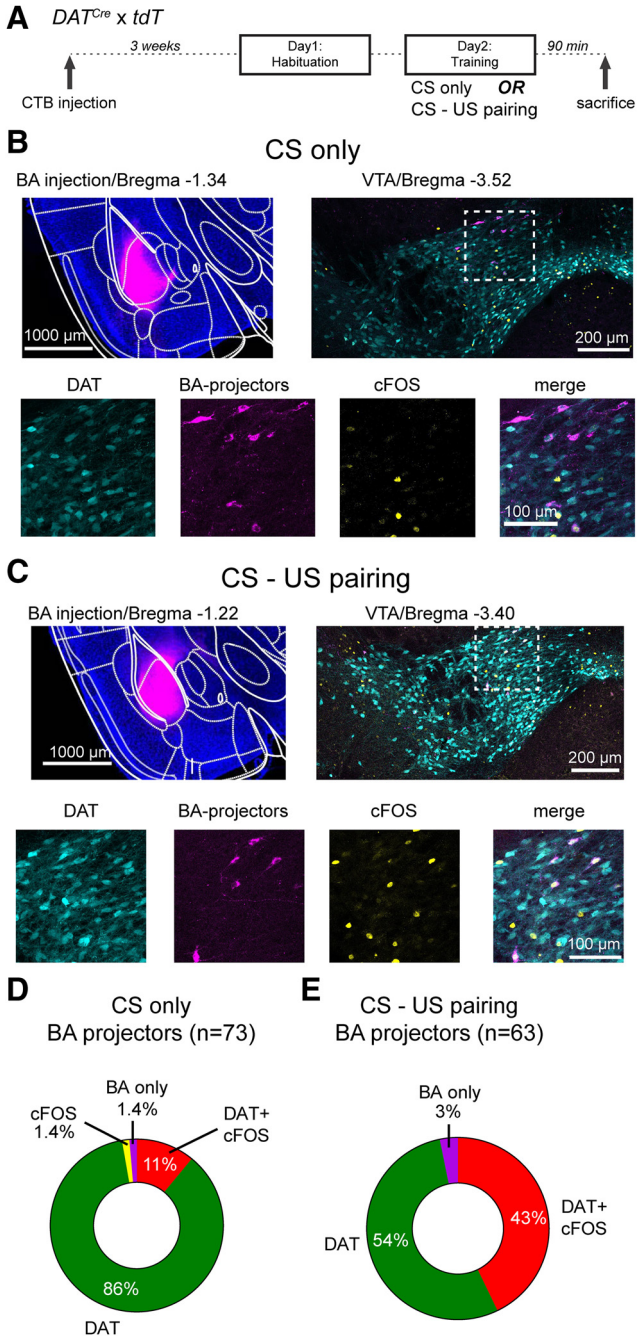

Figure 3. Combined cfos labeling and retrograde tracing show that BA projectors increase their activity during tone-footshock pairing. ***A***, Schematic of the protocol used for cfos labeling; 90 min after the training session, mice were killed and prepared for cfos immunohistochemistry. ***B***, Example images from a mouse that received only tones during the training on day 2 (CS only; control group). Top left, Wide-field fluorescence image of the BA injected with CTB-Alexa-647 for retrograde labeling (magenta channel). Top right, Confocal image on the level of the VTA, with tdTomato-positive DAT^+ neurons (cyan channel) as well as labeling by the cfos antibody (yellow channel) and by CTB-Alexa-647 (magenta). Bottom row, Images represent the individual and merged channels for the boxed area in the top right. ***C***, Corresponding images from a different mouse, which underwent CS-US pairing (i.e., with footshocks) during the training day. ***D***, Quantification of all CTB-labeled neurons (BA projectors; $n = 73$) and their colabeling in $N = 2$ mice in the control group. A large percentage of BA projectors is DAT^+ (the sum of DAT and DAT^+ cfos classes; 97%), but only 11% are stained by cfos. ***E***, Quantification of all CTB-labeled neurons (BA projectors; $n = 63$) from $N = 2$ mice that underwent the CS-US pairing before cfos immunohistochemistry. Note the larger percentage of DAT^+, $cfos^+$ BA projectors (43%; for statistical analysis, see Results).

control group). Ninety minutes later, the mice were killed and prepared for cfos immunohistochemistry (Fig. 3*A*).

Figure 3*B*, *C* shows example images for a control mouse (CS only), and for a CS-US pairing mouse. In both cases, the CTB injection was well targeted to the BA (Fig. 3*B*,*C*, top row, left). DAT^+ neurons in the VTA were identified by their tdTomato signal (Fig. 3*B*,*C*, cyan channel). Using confocal images, we then concentrated on identifying BA projectors based on their CTB-Alexa-647 fluorescence, and analyzed the colocalization with the other two markers (Fig. 3*B*,*C*; bottom row images). As before, the number of BA projectors was small ($n = 73$ and $n = 63$), analyzed from $n = 12$ and $n = 11$ sections from $N = 2$ control mice and $N = 2$ CS-US pairing mice, respectively. In the control mice, of the 73 BA projectors, there were only $n = 2$ non-DAT cells. Among these, one was not positive for cfos (Fig. 3*D*, BA only), the other one was a $cfos^+$ BA projector; these numbers correspond to 1.4% in each case (Fig. 3*D*). Of the $n = 73$ BA projectors in the control group, $n = 8$ (or 11%) were $cfos^+$ (Fig. 3*D*). Interestingly, this fraction was significantly increased (to 43%) in the CS-US pairing group (Fig. 3*E*; $\chi^2 = 14.26$; $p = 0.0002$; χ^2 test for trend). Similar to the control mice, the number of non-DAT BA projectors was also small in the CS-US pairing group (Fig. 3*E*; BA only; 3%). Together, the cfos labeling experiments show that BA projectors become significantly activated during CS-US pairing. Furthermore, the tdTomato fluorescence of DAT^+ cells shows that a majority (>95%) of the BA projectors are dopamine neurons. These results further corroborate the findings of the *in vivo* optrode recordings and suggest that BA projectors are among those units that show an increased AP firing in response to footshocks.

Role of VTA dopamine neurons in auditory-cued fear memory

To investigate whether dopamine neurons in the VTA contribute to the formation of an auditory-cued threat memory, we next used optogenetic methods. Because we found that many VTA neurons, including dopamine neurons (Fig. 2) and BA projectors (Fig. 3), increase their AP firing in response to footshocks, we wished to silence VTA dopamine neurons at the time of the footshock, and observe the effect on fear learning. For this, we used DAT^{Cre} mice, and expressed the light-activated proton pump Arch-eGFP in a Cre-dependent manner virally in the VTA (using AAV1:CBA:FLEX:Arch-eGFP; Fig. 4*A*). Initial slice electrophysiology showed that yellow light (561 nm) caused robust outward currents and strong hyperpolarization of Arch-expressing VTA dopamine neurons (Fig. 4*B*,*C*; $n = 5$ recordings from $N = 3$ mice).

We then tested whether VTA dopamine neuron firing during the footshock is needed for fear memory formation. We injected AAV1:CBA:FLEX:Arch-eGFP into the VTA of DAT^{Cre} mice and implanted a single optic fiber over the VTA (Fig. 4*D*,*E*; only a single fiber could be used because of the medial position of the VTA; see Materials and Methods). To ask whether footshock-driven firing of dopamine neurons was necessary for fear learning, yellow light was applied for 3 s starting 1 s before the footshock and ending 1 s after the footshock (Fig. 4*F*). Mice that received an AAV driving the Cre-dependent expression of eGFP (AAV1:CBA:FLEX:eGFP) in the VTA, but that otherwise underwent identical procedures as the Arch group, served as control mice. In these experiments, in addition to testing the retrieval of auditory-cued fear memory on day 3, we also tested the retrieval of contextual fear memories on a fourth day, using the same context as on day 1 and day 2 of the fear memory protocol (see Materials and Methods).

The average freezing levels of both groups of mice during the 4 d behavioral tests are shown in Figure 4*G*. A two-way repeated-measures ANOVA revealed a significant effect of silencing on the freezing levels during the fear learning protocol ($p = 0.0117$; $F_{(15,150)} = 2.12$ for the interaction between the two factors time, and photoinhibition). A *post hoc* Bonferroni test showed a significant difference in the freezing level for the sixth tone-footshock pairing on the training day ($p < 0.05$), and for the second and third tone block on the retrieval day ($p < 0.01$ for both; Fig. 4*G*). Pooling the freezing data over the four tone blocks of day 3 indicated a significantly reduced retrieval of cued threat memory ($p = 0.013$, *t* test; Fig. 4*H*). On the other hand, the contextual fear memory retrieval tested on day 4 was not significantly different between the Arch group and the eGFP group (Fig. 4*G*, right; $p = 0.102$, *t* test). Together, these results suggest that footshock-driven activity of VTA dopamine neurons on the training day contributes to the formation of auditory-cued fear memory.

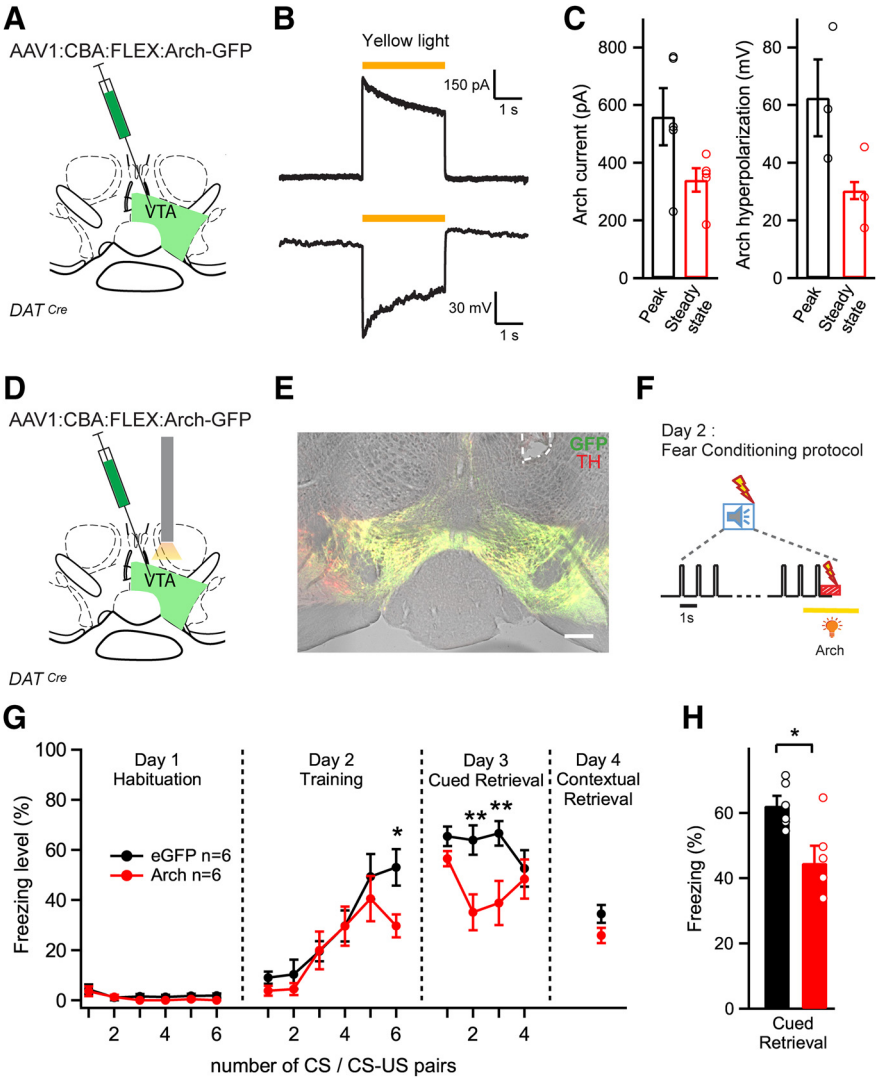

Figure 4. Optogenetic inhibition of VTA dopamine neurons during the footshock decreases auditory-cued fear memory. ***A***, Schematic of the experimental approach for ***B***, ***C***. An AAV1:CBA:FLEX:Arch-eGFP vector was injected unilaterally into the VTA. ***B***, Current (top; holding potential, −60 mV) and membrane potential responses (bottom) evoked by yellow light ($\lambda = 595$ nm) in an Arch-expressing DAT neuron. ***C***, Quantification of the peak and steady-state current response (left) and hyperpolarization (right) from $n = 5$ recordings in $N = 3$ mice. ***D***, Schematic of the experimental approach for ***E-H***. A stereotactic injection of the Cre-dependent Arch-eGFP vector into the VTA of DAT^{Cre} mice was followed by unilateral optic fiber implantation above the injection site. ***E***, *Post hoc* histologic verification of Arch-GFP expression and optic fiber placement (white dashed line) in the VTA of one example mouse. Red represents TH immunohistochemistry signal. Green represents fluorescence of Arch-eGFP. Scale bar, 200 μm. ***F***, Schematic of yellow laser light illumination during the CS-US pairing protocol. The tone block ($n = 30$ tone beeps of 0.1 s at 1 Hz) is followed by a 1 s footshock. Yellow laser light ($\lambda = 561$ nm) is applied for 3 s starting 1 s before the footshock to activate Arch. ***G***, Average time course of freezing level in Arch-expressing mice ($n = 6$, red), and in eGFP-expressing control mice ($n = 6$; black). *Significance of the photoinhibition effect as assessed by Bonferroni *post hoc* test at the indicated time points, following a two-way repeated-measures ANOVA. ***H***, Percentage of freezing during cued fear memory retrieval averaged over four CS presentations on day 3 ($N = 6$ and $N = 6$ mice in the test and control group; $p = 0.0134$, *t* test). One data point from a mouse in the control group showed unusually low freezing on retrieval (26%) and was removed from the dataset. Error bars indicate mean ± SEM. *$p < 0.05$, **$p < 0.01$.

The VTA to BA projection contributes to auditory-cued fear learning

The experiments of Figure 4 suggest that dopamine neurons in the VTA contribute to the formation of auditory-cued fear memories. Nevertheless, there are several projections of VTA dopamine neurons that might contribute to aversive learning, including projections to the mPFC and NAc (Vander Weele et al., 2018; de Jong et al., 2019), as well as the projection to the BA that we characterized anatomically and by cfos imaging (Figs. 1, 3). To study the role of the VTA to BA projection more specifically, we next silenced the axons of the VTA dopamine neurons in the BA. This was achieved by bilateral injection of AAV1:CBA:FLEX:Arch-eGFP into the VTA of DAT^{Cre} mice, and implantation of optic fibers bilaterally over each BA (Fig. 5*A*,*B*). Mice injected with an AAV vector that drives the expression of eGFP in the VTA served as a control group. Yellow light (561 nm) was again delivered during a 3 s period centered over the footshock stimulation on the training day (Fig. 5*C*).

In the Arch group, we found a significant difference of freezing across the fear learning protocol compared with the eGFP group (Fig. 5*D*; $F_{(15,195)} = 1.87$, $p = 0.0238$, for interaction between photoinhibition and time; two-way repeated-measures ANOVA). Bonferroni *post hoc* analysis showed that freezing in response to the fourth tone block on the retrieval day was significantly reduced ($p < 0.05$). Analysis of the pooled data over all four tone blocks of the retrieval day showed a significant decrease of freezing in the Arch group compared with the eGFP group (Fig. 5*E*; $p = 0.0043$, *t* test). Furthermore, contextual fear memory retrieval tested on day 4 was significantly different in Arch-eGFP-expressing mice compared with the control group (Fig. 5*D*, right; $p = 0.046$, *t* test). These data show that footshock-driven activity of VTA DAT^{+} axons in the BA contributes to the formation of auditory-cued fear memories, as well as to the formation of contextual fear memories.

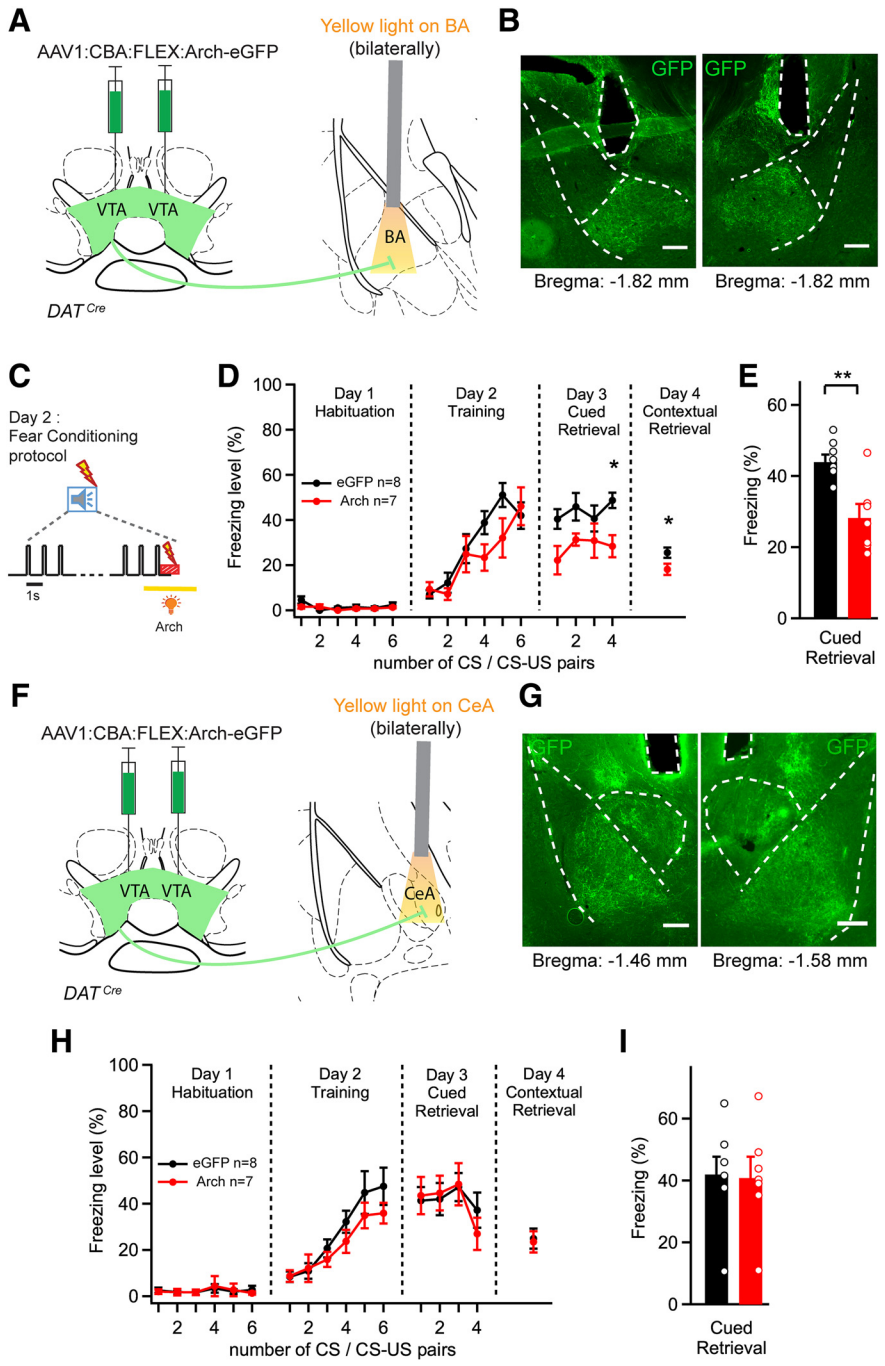

Fig. 5. Photoinhibition of the dopaminergic projection from the VTA to the BA during the footshock decreases the amount of cued and contextual fear memory. ***A***, Schematic of the experimental approach for ***B–E***. An AAV1:CBA:FLEX:Arch-eGFP vector was injected bilaterally into the VTA of DAT^{Cre} mice, and optical fibers were implanted above each BA. ***B***, *Post hoc* histologic validation of the bilateral optical fiber implantation above the BA. Scale bar, 200 μm. ***C***, Scheme of the timing of yellow light application (561 nm, 3 s) delivered to each BA, aimed to suppress footshock-driven activity of VTA axons in the BA. ***D***, Average time courses of freezing in Arch-eGFP-expressing mice (red data points) and in eGFP-expressing control mice (black). *Statistical significance of photoinhibition effect assessed by Bonferroni *post hoc* test for multiple comparisons at the respective time points, following the two-way repeated-measures ANOVA. ***E***, Percentage of freezing during cued fear retrieval on day 3, averaged over the four CS presentations ($N = 8$ and $N = 7$ mice in the control and test group, respectively; $p = 0.0043$; *t* test). ***F***, Experimental approach for ***G–I***, in which optical fibers were implanted bilaterally above each CeA. ***G***, *Post hoc* histologic validation of the bilateral optical fiber implantation above each CeA in 1 mouse. Scale bar, 200 μm. ***H***, ***I***, Time course and average freezing levels after silencing the VTA dopaminergic fibers over the CeA. There was no significant difference between the Arch and the eGFP (control) group (two-way repeated-measures ANOVA in ***H*** and *t* test in ***I***; $p = 0.9$). Error bars indicate mean ± SEM. *$p < 0.05$, **$p < 0.01$.

Because we found that VTA dopamine neurons also project to the CeA and especially to the medial division of the CeA (Fig. 1) (Mingote et al., 2015), we next tested whether this pathway might contribute to auditory-cued fear learning. We again expressed Arch-eGFP Cre-dependently bilaterally in the VTA of DAT^{Cre} mice (using AAV1:CBA:FLEX:Arch-eGFP), but we now implanted optic fibers bilaterally over each CeA (Fig. 5*F*,*G*). Yellow light was applied for 3 s during the footshock stimuli. ANOVA did not find a significant effect of silencing on freezing (Fig. 5*H*; $F_{(15,195)} = 0.6$, $p = 0.875$ for interaction between photoinhibition and time; two-way repeated-measures ANOVA). Similarly, pooling of the freezing data on the retrieval day did not reveal a significant difference between the groups (Fig. 5*I*; $p = 0.90$, *t* test). Finally, the contextual retrieval of fear memories on day 4 was not significantly different after silencing the dopaminergic VTA axons over the CeA (Fig. 5*H*, right; $p = 0.83$, *t* test). Together, the experiments in Figure 5 show that the dopaminergic VTA to BA pathway contributes to the formation of auditory-cued threat memories and to contextual fear memories, whereas the VTA to CeA projection seems not necessary for these learning behaviors.

Discussion

Using *in vivo* optogenetic methods and optrode recordings, as well as anatomic circuit tracing and cfos imaging, we have studied the role of the VTA to BA dopamine pathway in the formation of an auditory-cued fear memory. We found that a sparse population of VTA dopamine neurons projects to the BA and becomes activated by footshocks. *In vivo* optrode recordings of single units in the VTA showed that most recorded units, including putative dopamine neurons, responded to the footshock with increased AP firing rates, and acquire CS responsiveness. Silencing the VTA-BA pathway during footshock presentation led to reduced fear memory as tested 1 day later, suggesting that footshock-driven activity of VTA axons in the BA facilitates the formation of an auditory-cued fear memory. Thus, we conclude that VTA dopamine neurons

contribute to signal salient somatosensory events to the BA, presumably by causing dopamine release, which facilitates the formation of a fear memory.

A role of dopamine in aversive learning has first been hypothesized based on pharmacological experiments with D1 and D2 receptor blockers and microdialysis-based dopamine measurements in the amygdala (Lamont and Kokkinidis, 1998; Young and Rees, 1998; Guarraci et al., 1999; Nader and LeDoux, 1999). Furthermore, fear-potentiated startle was reduced in the dopamine-deficient mouse model and after conditional genetic deletion of NMDA receptors in TH^+ neurons (Fadok et al., 2009; Zweifel et al., 2011). On the other hand, the generally accepted role of VTA dopamine neurons in reward processing (Schultz, 1998; Wise, 2004), and recordings that showed an inhibition of AP firing of VTA dopamine neurons by aversive stimuli (Ungless et al., 2004; Tan et al., 2012), might have slowed progress in understanding the role of dopamine in aversively motivated learning. More recent circuit tracing analyses showed that the VTA is composed of neurons with diverse projection areas belonging to different subsystems (Lammel et al., 2011, 2012; Beier et al., 2015). These dopaminergic subsystems in the VTA can be involved in both reward-based learning (for most NAc projectors) or in aversive learning (mPFC projectors) (Lammel et al., 2011; Vander Weele et al., 2018). Nevertheless, the VTA to amygdala pathway had received little attention in recent studies.

Using *in vivo* optrode recordings in the VTA throughout the 3 day fear learning protocol, we found that most recorded units, including putative dopamine neurons identified optogenetically, increased their AP firing in response to footshocks (Fig. 2). Even within the sample of putative DAT^+ neurons, we only found a single unit that was inhibited by the footshock (Fig. 2). Furthermore, we found that a population of units that largely overlapped with the US-responsive units developed a response to tones when these were reinforced by the footshock (Fig. 2). This CS learning might be caused by plasticity of excitatory synapses on VTA dopamine neurons which was previously observed after drugs of abuse (Ungless et al. 2001), but also after pain stimuli and after fear learning (Lammel et al. 2011; Pignatelli et al. 2017). Although we could not identify BA projectors in these *in vivo* recordings, further cfos imaging showed that BA projectors in the VTA become activated by sound-footshock pairings, and that >95% of the BA projectors are DAT^+ neurons (Fig. 3). These findings provide further evidence for the notion that dopaminergic BA projectors in the VTA are activated by footshocks, and contribute to auditory-cued fear learning.

It was shown, largely based on AP waveform criteria, that footshocks in anesthetized mice excite putative VTA GABA neurons, and mostly inhibit putative VTA dopamine neurons (Tan et al., 2012). It remains possible that a fraction of the nonidentified units in our sample of optrode recordings represented GABA neurons. On the other hand, we found that non-DAT^+ neurons were a minority (~3%) of the histologically identified BA projectors (Fig. 3). Furthermore, our optogenetic results showed that inhibition of VTA dopamine neurons during the footshock, as well as inhibition of VTA dopamine axons in the BA, each significantly reduced threat memory formation (Figs. 4, 5). These results strongly suggest that footshocks activate dopamine neurons in the VTA, and that the resulting release of dopamine in the BA facilitates fear memory formation.

Several recent studies have provided evidence for roles of distinct dopamine neuron populations, both within the VTA and in adjacent midbrain areas, in aversively motivated learning. One study found that VTA dopaminergic axons that project to a ventromedial area of the NAc shell were excited by footshocks (de Jong et al., 2019). Interestingly, these axons acquired a tone response when the latter was paired with footshocks, similar to what we found here for a large fraction of recorded VTA units (Fig. 2). De Jong et al. (2019) also showed that projections to the lateral shell of the NAc (these dopamine axons were involved in reward processing) were inhibited by footshocks. Yet another population of VTA dopamine neurons, the mPFC projectors, are involved in aversive valence processing (Lammel et al., 2011; Vander Weele et al., 2018). Thus, in addition to the VTA dopamine neurons projecting to the BA that we have studied here, there are other populations of VTA dopamine neurons projecting to other targets, which are involved in aversively motivated learning. Furthermore, dopamine neurons located in the dorsal raphe that project to the CeA, and dopamine neurons of the lateral portion of the substantia nigra that project to the posterior striatum, were recently shown to be involved in aversive learning (Groessl et al., 2018; Menegas et al., 2018). Different molecularly defined subpopulations of dopamine neurons innervating the various forebrain areas have recently been identified using intersectional genetic approaches (Poulin et al., 2018). Together, these functional and genetic circuit studies corroborate the anatomic notion that distinct populations of midbrain dopamine neurons have largely separate projection targets (Swanson, 1982; Menegas et al., 2015). The various dopamine projection pathways that are involved in aversive learning might be regarded as parallel streams of neuromodulatory input to largely separate projection domains in the forebrain. The functional advantage for such parallel streams of dopamine signaling should be further elaborated in future work.

We have found a contribution of the VTA-BA dopamine projection to the formation of auditory-cued threat memories (Fig. 5). These findings support the notion that dopamine contributes to a "teaching" signal for plasticity in the BA (Herry and Johansen, 2014). On the other hand, the LA, which receives many sensory inputs from cortical and thalamic areas (LeDoux et al., 1990; Nabavi et al., 2014; Lucas et al., 2016), was only sparsely innervated by dopamine fibers from the VTA (Fig. 1). Correspondingly, we have focused on the role of the VTA-BA dopamine pathway in fear learning. A recent study showed that the VTA to CeA dopamine pathway is involved in discriminative fear learning, as apparent by a dopamine-dependent *reduction* of freezing in response to a nonreinforced tone (Jo et al., 2018). Interestingly, the learned freezing in response to a reinforced tone was not strongly affected by silencing the VTA-CeA dopamine pathway, consistent with our results (Fig. 5*F*), but the previous study used footshocks with lower intensity. Thus, the VTA-CeA connection does not seem to play a significant role in basic forms of auditory-cued fear learning but is relevant for discriminative fear learning (Jo et al., 2018).

What might be the mechanisms by which dopamine acts in the BA to promote fear memory formation? Dopamine acts on metabotropic D1- and D2-like receptors (Neve et al., 2004; Tritsch and Sabatini, 2012), and activation of both D1 and D2 receptor subtypes in the amygdala (Lamont and Kokkinidis, 1998; Guarraci et al., 2000) is expected to modulate various signaling pathways. These include an upregulation of intrinsic neuronal excitability via D1 receptors (Kroner et al., 2005; Tang, 2018), a D2 receptor-mediated decrease in neurotransmitter release at both excitatory and inhibitory nerve terminals (Rosenkranz and Grace, 1999; Chu et al., 2012), and an action of D1 receptors on intracellular signaling pathways involved in long-term plasticity

of excitatory synapses (Li et al., 2011). It is likely that these separate, but synergistically acting mechanisms, including a possible dopamine-mediated disinhibition of principal cells (Bissiere et al., 2003; Chu et al., 2012), together facilitate the induction of plasticity at excitatory synapses in the BA during fear learning.

In conclusion, our study shows that a sparse population of dopamine neurons in the VTA projects to the BA and becomes activated during tone-footshock pairing. Optogenetic silencing of this projection demonstrates a contribution of the VTA to BA pathway in the formation of auditory-cued fear memories. Understanding how dopamine acts as a teaching signal in aversively motivated learning will allow us to gain further insights into the mechanisms of maladaptive plasticities that underlie anxiety and post-traumatic stress disorder (Yeh et al., 2018).

References

Amano T, Duvarci S, Popa D, Paré D (2011) The fear circuit revisited: contributions of the basal amygdala nuclei to conditioned fear. J Neurosci 31:15481–15489.

Anikeeva P, Andalman AS, Witten I, Warden M, Goshen I, Grosenick L, Gunaydin LA, Frank LM, Deisseroth K (2011) Optetrode: a multichannel readout for optogenetic control in freely moving mice. Nat Neurosci 15:163–170.

Asan E (1998) The catecholaminergic innervation of the rat amygdala. Adv Anat Embryol Cell Biol 142:1–118.

Bäckman CM, Malik N, Zhang Y, Shan L, Grinberg A, Hoffer BJ, Westphal H, Tomac AC (2006) Characterization of a mouse strain expressing Cre recombinase from the 3′ untranslated region of the dopamine transporter locus. Genesis 44:383–390.

Baimel C, Lau BK, Qiao M, Borgland SL (2017) Projection-target-defined effects of orexin and dynorphin on VTA dopamine neurons. Cell Rep 18:1346–1355.

Beier KT, Steinberg EE, DeLoach KE, Xie S, Miyamichi K, Schwarz L, Gao XJ, Kremer EJ, Malenka RC, Luo L (2015) Circuit architecture of VTA dopamine neurons revealed by systematic input-output mapping. Cell 162:622–634.

Bissiere S, Humeau Y, Luthi A (2003) Dopamine gates LTP induction in lateral amygdala by suppressing feedforward inhibition. Nat Neurosci 6:587–592.

Brischoux F, Chakraborty S, Brierley DI, Ungless MA (2009) Phasic excitation of dopamine neurons in ventral VTA by noxious stimuli. Proc Natl Acad Sci USA 106:4894–4899.

Chu HY, Ito W, Li J, Morozov A (2012) Target-specific suppression of GABA release from parvalbumin interneurons in the basolateral amygdala by dopamine. J Neurosci 32:14815–14820.

Davis M (1992) The role of the amygdala in fear and anxiety. Annu Rev Neurosci 15:353–375.

de Jong JW, Afjei SA, Pollak Dorocic I, Peck JR, Liu C, Kim CK, Tian L, Deisseroth K, Lammel S (2019) A neural circuit mechanism for encoding aversive stimuli in the mesolimbic dopamine system. Neuron 101:133–151.e137.

de Oliveira AR, Reimer AE, de Macedo CE, de Carvalho MC, Silva MA, Brandão ML (2011) Conditioned fear is modulated by D2 receptor pathway connecting the ventral tegmental area and basolateral amygdala. Neurobiol Learn Mem 95:37–45.

Duvarci S, Paré D (2014) Amygdala microcircuits controlling learned fear. Neuron 82:966–980.

Fadok JP, Dickerson TM, Palmiter RD (2009) Dopamine is necessary for cue-dependent fear conditioning. J Neurosci 29:11089–11097.

Feinberg TE, Mallatt JM (2017) The ancient origins of consciousness: how the brain created experience. Cambridge, MA: Massachusetts Institute of Technology.

Franklin KB, Paxinos G (2016) The mouse brain in stereotaxic coordinates, Ed 4. San Diego: Elsevier/Academic.

Gore BB, Soden ME, Zweifel LS (2014) Visualization of plasticity in fear-evoked calcium signals in midbrain dopamine neurons. Learn Mem 21:575–579.

Gore F, Schwartz EC, Brangers BC, Aladi S, Stujenske JM, Likhtik E, Russo MJ, Gordon JA, Salzman CD, Axel R (2015) Neural representations of unconditioned stimuli in basolateral amygdala mediate innate and learned responses. Cell 162:134–145.

Grewe BF, Gründemann J, Kitch LJ, Lecoq JA, Parker JG, Marshall JD, Larkin MC, Jercog PE, Grenier F, Li JZ, Lüthi A, Schnitzer MJ (2017) Neural ensemble dynamics underlying a long-term associative memory. Nature 543:670–675.

Groessl F, Munsch T, Meis S, Griessner J, Kaczanowska J, Pliota P, Kargl D, Badurek S, Kraitsy K, Rassoulpour A, Zuber J, Lessmann V, Haubensak W (2018) Dorsal tegmental dopamine neurons gate associative learning of fear. Nat Neurosci 21:952–962.

Guarraci FA, Kapp BS (1999) An electrophysiological characterization of ventral tegmental area dopaminergic neurons during differential pavlovian fear conditioning in the awake rabbit. Behav Brain Res 99:169–179.

Guarraci FA, Frohardt RJ, Kapp BS (1999) Amygdaloid D1 dopamine receptor involvement in Pavlovian fear conditioning. Brain Res 827:28–40.

Guarraci FA, Frohardt RJ, Falls WA, Kapp BS (2000) The effects of intra-amygdaloid infusions of a D2 dopamine receptor antagonist on Pavlovian fear conditioning. Behav Neurosci 114:647–651.

Hasue RH, Shammah-Lagnado SJ (2002) Origin of the dopaminergic innervation of the central extended amygdala and accumbens shell: a combined retrograde tracing and immunohistochemical study in the rat. J Comp Neurol 454:15–33.

Heath FC, Jurkus R, Bast T, Pezze MA, Lee JL, Voigt JP, Stevenson CW (2015) Dopamine D1-like receptor signalling in the hippocampus and amygdala modulates the acquisition of contextual fear conditioning. Psychopharmacology (Berl) 232:2619–2629.

Herry C, Johansen JP (2014) Encoding of fear learning and memory in distributed neuronal circuits. Nat Neurosci 17:1644–1654.

Horvitz JC (2000) Mesolimbocortical and nigrostriatal dopamine responses to salient non-reward events. Neuroscience 96:651–656.

Inglis FM, Moghaddam B (1999) Dopaminergic innervation of the amygdala is highly responsive to stress. J Neurochem 72:1088–1094.

Jiang L, Kundu S, Lederman JD, Lopez-Hernandez GY, Ballinger EC, Wang S, Talmage DA, Role LW (2016) Cholinergic signaling controls conditioned fear behaviors and enhances plasticity of cortical-amygdala circuits. Neuron 90:1057–1070.

Jo YS, Heymann G, Zweifel LS (2018) Dopamine neurons reflect the uncertainty in fear generalization. Neuron 100:916–925.e913.

Johansen JP, Diaz-Mataix L, Hamanaka H, Ozawa T, Ycu E, Koivumaa J, Kumar A, Hou M, Deisseroth K, Boyden ES, LeDoux JE (2014) Hebbian and neuromodulatory mechanisms interact to trigger associative memory formation. Proc Natl Acad Sci USA 111:E5584–E5592.

Kroner S, Rosenkranz JA, Grace AA, Barrionuevo G (2005) Dopamine modulates excitability of basolateral amygdala neurons in vitro. J Neurophysiol 93:1598–1610.

Lammel S, Ion DI, Roeper J, Malenka RC (2011) Projection-specific modulation of dopamine neuron synapses by aversive and rewarding stimuli. Neuron 70:855–862.

Lammel S, Lim BK, Ran C, Huang KW, Betley MJ, Tye KM, Deisseroth K, Malenka RC (2012) Input-specific control of reward and aversion in the ventral tegmental area. Nature 491:212–217.

Lamont EW, Kokkinidis L (1998) Infusion of the dopamine D1 receptor antagonist SCH 23390 into the amygdala blocks fear expression in a potentiated startle paradigm. Brain Res 795:128–136.

LeDoux JE (2000) Emotion circuits in the brain. Annu Rev Neurosci 23:155–184.

LeDoux JE, Cicchetti P, Xagoraris A, Romanski LM (1990) The lateral amygdaloid nucleus: sensory interface of the amygdala in fear conditioning. J Neurosci 10:1062–1069.

Li C, Dabrowska J, Hazra R, Rainnie DG (2011) Synergistic activation of dopamine D1 and TrkB receptors mediate gain control of synaptic plasticity in the basolateral amygdala. PLoS One 6:e26065.

Lucas EK, Jegarl AM, Morishita H, Clem RL (2016) Multimodal and site-specific plasticity of amygdala parvalbumin interneurons after fear learning. Neuron 91:629–643.

Madisen L, Zwingman TA, Sunkin SM, Oh SW, Zariwala HA, Gu H, Ng LL, Palmiter RD, Hawrylycz MJ, Jones AR, Lein ES, Zeng H (2010) A robust and high-throughput Cre reporting and characterization system for the whole mouse brain. Nat Neurosci 13:133–140.

Madisen L, Mao T, Koch H, Zhuo JM, Berenyi A, Fujisawa S, Hsu YW, Garcia AJ, Gu X, Zanella S, Kidney J, Gu H, Mao Y, Hooks BM, Boyden ES, Buzsáki G, Ramirez JM, Jones AR, Svoboda K, Han X, et al. (2012) A

toolbox of Cre-dependent optogenetic transgenic mice for light-induced activation and silencing. Nat Neurosci 15:793–802.
Matthews GA, Nieh EH, Vander Weele CM, Halbert SA, Pradhan RV, Yosafat AS, Glober GF, Izadmehr EM, Thomas RE, Lacy GD, Wildes CP, Ungless MA, Tye KM (2016) Dorsal raphe dopamine neurons represent the experience of social isolation. Cell 164:617–631.
Menegas W, Akiti K, Amo R, Uchida N, Watabe-Uchida M (2018) Dopamine neurons projecting to the posterior striatum reinforce avoidance of threatening stimuli. Nat Neurosci 21:1421–1430.
Menegas W, Bergan JF, Ogawa SK, Isogai Y, Umadevi Venkataraju K, Osten P, Uchida N, Watabe-Uchida M (2015) Dopamine neurons projecting to the posterior striatum form an anatomically distinct subclass. eLife 4: e10032.
Mingote S, Chuhma N, Kusnoor SV, Field B, Deutch AY, Rayport S (2015) Functional connectome analysis of dopamine neuron glutamatergic connections in forebrain regions. J Neurosci 35:16259–16271.
Mirenowicz J, Schultz W (1996) Preferential activation of midbrain dopamine neurons by appetitive rather than aversive stimuli. Nature 379:449–451.
Nabavi S, Fox R, Proulx CD, Lin JY, Tsien RY, Malinow R (2014) Engineering a memory with LTD and LTP. Nature 511:348–352.
Nader K, LeDoux JE (1999) Inhibition of the mesoamygdala dopaminergic pathway impairs the retrieval of conditioned fear associations. Behav Neurosci 113:891–901.
Nelson EL, Liang CL, Sinton CM, German DC (1996) Midbrain dopaminergic neurons in the mouse: computer-assisted mapping. J Comp Neurol 369:361–371.
Neve KA, Seamans JK, Trantham-Davidson H (2004) Dopamine receptor signaling. J Recept Signal Transduct Res 24:165–205.
Newman JP, Fong MF, Millard DC, Whitmire CJ, Stanley GB, Potter SM (2015) Optogenetic feedback control of neural activity. eLife 4:e07192.
Pignatelli M, Umanah GKE, Ribeiro SP, Chen R, Karuppagounder SS, Yau HJ, Eacker S, Dawson VL, Dawson TM, Bonci A (2017) Synaptic Plasticity onto Dopamine Neurons Shapes Fear Learning. Neuron 93:425–440.
Poulin JF, Caronia G, Hofer C, Cui Q, Helm B, Ramakrishnan C, Chan CS, Dombeck DA, Deisseroth K, Awatramani R (2018) Mapping projections of molecularly defined dopamine neuron subtypes using intersectional genetic approaches. Nat Neurosci 21:1260–1271.
Quirk GJ, Repa C, LeDoux JE (1995) Fear conditioning enhances short-latency auditory responses of lateral amygdala neurons: parallel recordings in the freely behaving rat. Neuron 15:1029–1039.
Rosenkranz JA, Grace AA (1999) Modulation of basolateral amygdala neuronal firing and afferent drive by dopamine receptor activation in vivo. J Neurosci 19:11027–11039.
Rossant C, Kadir SN, Goodman DF, Schulman J, Hunter ML, Saleem AB, Grosmark A, Belluscio M, Denfield GH, Ecker AS, Tolias AS, Solomon S, Buzsaki G, Carandini M, Harris KD (2016) Spike sorting for large, dense electrode arrays. Nat Neurosci 19:634–641.
Rothman JS, Silver RA (2018) NeuroMatic: an integrated open-source software toolkit for acquisition, analysis and simulation of electrophysiological data. Front Neuroinform 12:14.
Rumpel S, LeDoux J, Zador A, Malinow R (2005) Postsynaptic receptor trafficking underlying a form of associative learning. Science 308:83–88.
Schmitzer-Torbert N, Jackson J, Henze D, Harris K, Redish AD (2005) Quantitative measures of cluster quality for use in extracellular recordings. Neuroscience 131:1–11.
Schultz W (1998) Predictive reward signal of dopamine neurons. J Neurophysiol 80:1–27.
Sigurdsson T, Doyere V, Cain CK, LeDoux JE (2007) Long-term potentiation in the amygdala: a cellular mechanism of fear learning and memory. Neuropharmacology 52:215–227.
Sparta DR, Stamatakis AM, Phillips JL, Hovelso N, van Zessen R, Stuber GD (2011) Construction of implantable optical fibers for long-term optogenetic manipulation of neural circuits. Nat Protoc 7:12–23.
Swanson LW (1982) The projections of the ventral tegmental area and adjacent regions: a combined fluorescent retrograde tracer and immunofluorescence study in the rat. Brain Res Bull 9:321–353.
Tan KR, Yvon C, Turiault M, Mirzabekov JJ, Doehner J, Labouebe G, Deisseroth K, Tye KM, Lüscher C (2012) GABA neurons of the VTA drive conditioned place aversion. Neuron 73:1173–1183.
Tang W (2018) The dopaminergic VTA-basal amygdala projection contributes to signal aversive state in fear memory. PhD thesis, Ecole Polytechnique Fédérale de Lausanne.
Tovote P, Fadok JP, Lüthi A (2015) Neuronal circuits for fear and anxiety. Nat Rev Neurosci 16:317–331.
Tritsch NX, Sabatini BL (2012) Dopaminergic modulation of synaptic transmission in cortex and striatum. Neuron 76:33–50.
Uematsu A, Tan BZ, Ycu EA, Cuevas JS, Koivumaa J, Junyent F, Kremer EJ, Witten IB, Deisseroth K, Johansen JP (2017) Modular organization of the brainstem noradrenaline system coordinates opposing learning states. Nat Neurosci 20:1602–1611.
Ungless MA, Whistler JL, Malenka RC, Bonci A (2001) Single cocaine exposure in vivo induces long-term potentiation in dopamine neurons. Nature 411:583–587.
Ungless MA, Magill PJ, Bolam JP (2004) Uniform inhibition of dopamine neurons in the ventral tegmental area by aversive stimuli. Science 303:2040–2042.
Vander Weele CM, Siciliano CA, Matthews GA, Namburi P, Izadmehr EM, Espinel IC, Nieh EH, Schut EH, Padilla-Coreano N, Burgos-Robles A, Chang CJ, Kimchi EY, Beyeler A, Wichmann R, Wildes CP, Tye KM (2018) Dopamine enhances signal-to-noise ratio in cortical-brainstem encoding of aversive stimuli. Nature 563:397–401.
Wise RA (2004) Dopamine, learning and motivation. Nat Rev Neurosci 5:483–494.
Yeh LF, Watanabe M, Sulkes-Cuevas J, Johansen JP (2018) Dysregulation of aversive signaling pathways: a novel circuit endophenotype for pain and anxiety disorders. Curr Opin Neurobiol 48:37–44.
Young AM, Rees KR (1998) Dopamine release in the amygdaloid complex of the rat, studied by brain microdialysis. Neurosci Lett 249:49–52.
Zweifel LS, Fadok JP, Argilli E, Garelick MG, Jones GL, Dickerson TM, Allen JM, Mizumori SJ, Bonci A, Palmiter RD (2011) Activation of dopamine neurons is critical for aversive conditioning and prevention of generalized anxiety. Nat Neurosci 14:620–626.